Cell Centered and Cell Vertex Multigrid Schemes for the Navier-Stokes Equations

R. C. Swanson*
NASA Langley Research Center, Hampton, Virginia 23665
and
R. Radespiel†
DLR, Institute for Design Aerodynamics, Braunschweig, Germany

Two efficient and robust finite-volume multigrid schemes for solving the Navier-Stokes equations are investigated. These schemes employ either a cell centered or a cell vertex discretization technique. An explicit Runge-Kutta algorithm is used to advance the solution in time. Acceleration techniques are applied to obtain faster steady-state convergence. Accuracy and convergence of the schemes are examined. Computational results for transonic airfoil flows are essentially the same, even for a coarse mesh. Both schemes exhibit very good convergence rates for a broad range of artificial dissipation coefficients.

Introduction

THE recent success in the numerical solution of the Euler and Navier-Stokes equations for complex configurations, such as an airplane, demonstrates the progress that has been made in computational fluid dynamics. Nevertheless, a formidable challenge for improved algorithms that are efficient, accurate, and reliable remains. The need for such improvements is absolutely crucial if Navier-Stokes solvers are to be used on a routine basis in the flight vehicle design process.

In the current work, two efficient and robust finite-volume multigrid schemes for solving the Navier-Stokes equations are investigated. These schemes employ either a cell centered or a cell vertex discretization technique. A multistage time-stepping algorithm is used to advance the solution in time. Acceleration techniques are applied to obtain faster steady-state convergence. These methods include the following: 1) local time stepping, 2) variable coefficient implicit residual smoothing, and 3) multigrid. In this paper, these elements of the two multigrid schemes are discussed in detail. Particular attention is directed toward accuracy and convergence. Theoretical estimates of accuracy are obtained using Taylor series expansions. Numerical verification of accuracy is included. Representative asymptotic convergence rates are established for a range of artificial dissipation coefficients. Solutions for transonic airfoil flows computed with the multigrid schemes are compared.

Discretization Techniques

The integral form of the two-dimensional compressible Navier-Stokes equations can be written as

$$\frac{\partial}{\partial t}\iint_{\Omega} W\,dx\,dy + \int_{\partial\Omega}(F\,dy - G\,dx) = 0 \qquad (1a)$$

where

$$W = [\rho\ \rho u\ \rho v\ \rho E]^T \qquad (1b)$$

F and G are the total flux vectors, Ω is the domain of interest, and $\partial\Omega$ is the boundary of the domain. The quantity ρ is the density, u and v are the Cartesian velocity components, and E is the specific total internal energy. If the physical space is partitioned with quadrilaterals and Eq. (1) is applied to each cell, a set of discrete equations for the fluid motion is obtained. There are two basic finite-volume techniques for the discretization. One is a cell centered scheme, and the other is a cell vertex scheme.

With the cell centered (CC) scheme, the flow variables are located at the cell center (see Fig. 1a). The flux vectors at the midpoint of a cell face are evaluated by an averaging proce-

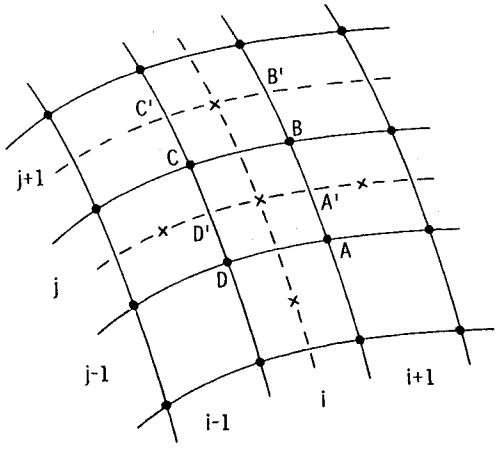

a) Cell centered scheme

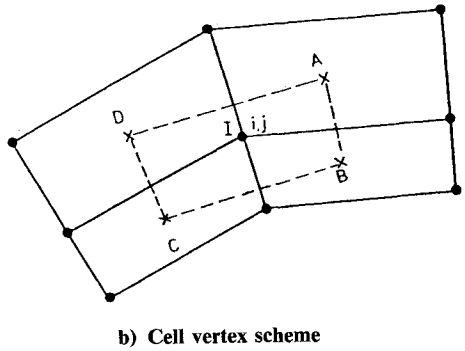

b) Cell vertex scheme

Fig. 1 Finite-volume discretization schemes.

Received May 19, 1989; revision received June 7, 1990; accepted for publication June 12, 1990.

*Research Scientist, Theoretical Flow Physics Branch, Fluid Mechanics Division. Member AIAA.
†Head of Aerothermodynamics Section.

dure. The line integral in Eq. (1) is approximated with the midpoint rule. To compute the shear stress and heat conduction terms, which involve first-order derivatives, Green's theorem is used. For example, the contributions u_x and u_y to the viscous flux across cell face BC, which is indicated in Fig. 1a, are determined using

$$\iint_{\Omega'} u_x \, d\Omega' = \int_{\partial\Omega'} u \, dy \tag{2a}$$

$$\iint_{\Omega'} u_y \, d\Omega' = -\int_{\partial\Omega'} u \, dx \tag{2b}$$

where Ω' is the auxiliary cell $A'B'C'D'$. The values of u at B and C required for the cell boundary integrals in Eqs. (2) are obtained by a simple average of the values of u at the four surrounding cells. In a similar manner, v_x and v_y are computed. Additional details for finite-volume treatment of viscous stresses and heat conduction terms are found in Refs. 1 and 2. Note that in the current work, the thin-layer form (viscous transport processes in the streamwise direction neglected) of the Navier-Stokes equations is solved.

In the case of a cell vertex (CV) scheme, the flow variables are located at the vertices of the mesh cells. Consider a super cell, as depicted in Fig. 1b. The dependent variables at the midpoints of the faces of the four component cells of the super cell are obtained by averaging the values at adjacent vertices. The line integral of Eq. (1) is evaluated for each component cell with the trapezoidal rule. Then, the resultant convective inflow of mass, momentum, and energy associated with point i, j is computed by summing the contributions of the component cells. Next, the viscous fluxes required to determine the solution at the point i, j are approximated using the auxiliary cell with the dashed boundary shown in Fig. 1b. The viscous fluxes for each face of the auxiliary cell are calculated by applying the local transformation $(x,y)\rightarrow(\xi,\eta)$, where (x,y) are Cartesian coordinates and (ξ,η) are arbitrary curvilinear coordinates. That is,

$$\phi_x = \frac{\phi_\xi y_\eta - \phi_\eta y_\xi}{x_\xi y_\eta - x_\eta y_\xi} \tag{3}$$

where ϕ is any flow quantity, the derivative is evaluated at the midpoint of an auxiliary cell face, and the denominator is the averaged volume of the cells nearest to the face. Alternatively, one could evaluate the first derivatives at the centers of the component cells and then average them to obtain the viscous fluxes. In Ref. 3, it was shown that this strategy decouples odd and even points on grids with a cell aspect ratio of one, and may even amplify oscillations in the solution on grids with large aspect ratio.

Theoretical estimates of the order of accuracy of the CC and CV schemes are now introduced, based on one-dimensional analysis using Taylor series expansions. This simple analysis not only demonstrates the effects of stretching on numerical accuracy, but also indicates what the phrase "sufficiently smooth mesh" means. For the CC scheme, the coordinate grid around the location denoted by the index i is presented in Fig. 2a. Let ϕ be a test function. Then, the numerical values of the first and second derivatives of this function are given by

$$(\phi_x)_{\text{num}} = \frac{1}{2}\phi_x\frac{\Delta x_+ + \Delta x_-}{\Delta x} + \frac{1}{4}\phi_{xx}\frac{\Delta x_+^2 - \Delta x_-^2}{\Delta x} + O(\Delta x^2) \tag{4a}$$

$$(\phi_{xx})_{\text{num}}\frac{1}{2}\phi_{xx}\frac{\Delta x_+ + \Delta x_-}{\Delta x} + \frac{1}{6}\phi_{xxx}\frac{\Delta x_+^2 - \Delta x_-^2}{\Delta x} + \frac{1}{24}\phi_{xxxx}\frac{\Delta x_+^3 + \Delta x_-^3}{\Delta x} + O(\Delta x^3) \tag{4b}$$

where the derivatives in the expansions are evaluated at i. The approximations of Eqs. (4) are zeroth-order accurate on arbitrarily stretched meshes. However, assuming a constant stretching factor of the grid (i.e., $\beta = \Delta x_{++}/\Delta x = \text{const.}$), we obtain the following relations:

$$\Delta x_{--} = \Delta x(1/\beta), \qquad \Delta x_- = \frac{1}{2}\Delta x[1 + (1/\beta)] \tag{5a}$$

$$\Delta x_{++} = \Delta x\beta, \qquad \Delta x_+ = \frac{1}{2}\Delta x(1 + \beta) \tag{5b}$$

For viscous flows, grids with constant stretching factor β are often used. If these grids are refined by doubling the number of points

$$\beta_f = \sqrt{\beta_c} < 1 + (\beta_c - 1)/2 \qquad \beta \geq 1 \tag{6}$$

where the subscripts refer to fine and coarse grids. In order to estimate the error reduction when refining the stretched mesh, we take

$$\beta \approx 1 + C_\beta \Delta x \tag{7}$$

Then, if the quantities in Eqs. (5) and (7) are substituted into Eqs. (4)

$$(\phi_x)_{\text{num}} = \phi_x + \frac{1}{4}\phi_x(C_\beta\Delta x)^2 + \frac{1}{2}C_\beta\phi_{xx}\Delta x^2 + O(\Delta x^2) \tag{8a}$$

$$(\phi_{xx})_{\text{num}} = \phi_{xx} + \frac{1}{4}\phi_{xx}(C_\beta\Delta x)^2 + \frac{1}{3}C_\beta\phi_{xxx}\Delta x^2 + (1/12)\phi_{xxxx}\Delta x^2 + O(\Delta x^3) \tag{8b}$$

for $\Delta x \ll 1$. Thus, second-order accuracy is achieved for the inviscid and viscous terms in the flow equations on smoothly stretched meshes.

In the case of the CV scheme, the coordinate grid around i is presented in Fig. 2b. The numerical values of the first and second derivatives of the test function ϕ at i are as follows:

$$(\phi_x)_{\text{num}} = \phi_x + \frac{1}{2}\phi_{xx}(\Delta x_+ - \Delta x) + O(\Delta x^2) \tag{9a}$$

$$(\phi_{xx})_{\text{num}} = \phi_{xx} + \frac{1}{3}\phi_{xxx}(\Delta x_+ - \Delta x) + (1/12)\phi_{xxxx}\frac{\Delta x_+^3 + \Delta x^3}{\Delta x_+ + \Delta x} + O(\Delta x^3) \tag{9b}$$

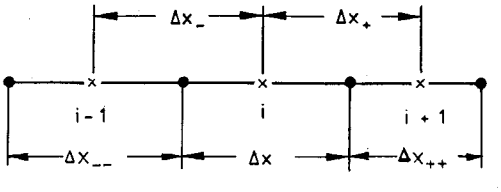

a) Three-point cell centered scheme

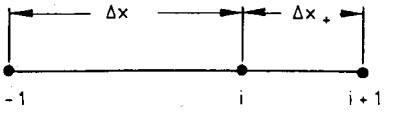

b) Three-point cell vertex scheme

Fig. 2 One-dimensional discretization schemes for derivatives.

The approximations of Eqs. (9) are first-order accurate on general stretched meshes. If the constant stretching factor β is introduced and Eq. (7) is applied, the expansions for the derivatives are defined by

$$(\phi_x)_{\text{num}} = \phi_x + \frac{1}{2} C_\beta \phi_{xx} \Delta x^2 + O(\Delta x^2) \tag{10a}$$

$$(\phi_{xx})_{\text{num}} = \phi_{xx} + \frac{1}{3} C_\beta \phi_{xxx} \Delta x^2 + (1/12)\phi_{xxxx} \Delta x^2 + (\Delta x^3) \tag{10b}$$

Therefore, the numerical accuracy for the CV scheme is also second-order for smoothly stretched meshes.

A two-dimensional analysis of estimates for first derivatives obtained with the CC and CV schemes is given by Morton and Paisley.[4] For the CC formulation, the ratio of the lengths of successive cell faces must be $1 + O(h)$ and $1 + O(h^2)$, where h characterizes the mesh spacing, for first-order and second-order accuracy, respectively. In the case of the CV scheme, this ratio must only be $1 + O(h)$ for a second-order approximation, and first-order accuracy is obtained even when the ratio is $1 + O(1)$. Even though this analysis and that given here clearly indicate the higher formal accuracy of the CV scheme on nonuniform meshes, one must also consider other factors in evaluating these schemes. For example, the numerical dissipation model may not allow adequate accuracy on the very meshes where the CV scheme would exhibit higher accuracy.

Boundary Conditions

At subsonic inflow and outflow boundaries, both the CC and CV schemes employ boundary point procedures that are based on characteristic theory. In the case of a lifting airfoil, the undisturbed freestream outside the computational domain is obtained by superimposing the flowfield of a single vortex to the onset flow.

At solid walls, the no-slip condition is enforced for viscous flows. With the CC scheme, the surface values of pressure p and temperature T are computed using the reduced normal momentum and energy equations

$$\frac{\partial p}{\partial \eta} = 0, \qquad \frac{\partial T}{\partial \eta} = 0 \tag{11}$$

where η is the coordinate normal to the surface. This approach for calculating the thermodynamic state variables at the wall resulted in a significant slowdown in convergence when used with the CV multigrid scheme. To overcome this difficulty, the continuity and energy equations are solved to obtain the density and temperature at the surface grid points. In particular, the control volume to update the wall quantities is formed with the two nearest cells outside the wall and their mirror images inside. When updating the convective terms, the flow variables at the computational points inside are obtained as the symmetric images of the values just outside. For the viscous terms, the velocity components inside are taken as the antisymmetric images of the values just outside.

Artificial Dissipation

For inviscid flows, the finite-volume schemes just described do not contain any dissipative terms. To prevent odd-even point decoupling and oscillations near shock waves or stagnation points, artificial dissipation terms are added to the governing discrete equations. For viscous flows (i.e., boundary layers, wakes), dissipative properties are present due to diffusive terms. However, due to nonlinear effects, the physical dissipation may not be sufficient to guarantee stability, especially in the case of the highly stretched meshes generally used to resolve the steep gradients in shear layers. Thus, to maintain the stability and robustness of the numerical procedure, artificial dissipation is also included in viscous regions. A semidiscrete form of Eqs. (1) is then given by

$$\frac{\mathrm{d}}{\mathrm{d}t}(\Omega \cdot W) + Q(W) - D(W) = 0 \tag{12}$$

where Ω is the area of the mesh cell being considered and will subsequently be assumed to be independent of time, $Q(W)$ represents the discrete approximation to the convective and physical diffusive terms, and $D(W)$ denotes the artificial dissipative terms.

The artificial dissipation model considered in this paper is basically the one developed by Jameson et al.[5] This nonlinear model is a blending of second and fourth differences. The quantity $D(W)$ in Eq. (12) is defined as

$$D(W) = (D_\xi^2 - D_\xi^4 + D_\eta^2 - D_\eta^4) W_{i,j} \tag{13}$$

where (ξ,η) are arbitrary curvilinear coordinates

$$D_\xi^2 W_{i,j} = \nabla_\xi \left[(\lambda_{i+\frac{1}{2},j} \epsilon^{(2)}_{i+\frac{1}{2},j}) \Delta_\xi \right] W_{i,j} \tag{14}$$

$$D_\xi^4 W_{i,j} = \nabla_\xi \left[(\lambda_{i+\frac{1}{2},j} \epsilon^{(4)}_{i+\frac{1}{2},j}) \Delta_\xi \nabla_\xi \Delta_\xi \right] W_{i,j} \tag{15}$$

where i, j are indices (associated with the ξ and η directions) referring to the location where the flow variables are stored, and Δ_ξ, ∇_ξ are forward and backward difference operators in the ξ direction. Following Refs. 2 and 6, the variable scaling factor is defined as

$$\lambda_{i+\frac{1}{2},j} = \frac{1}{2} [(\bar{\lambda}_\xi)_{i,j} + (\bar{\lambda}_\xi)_{i+1,j}] \tag{16}$$

where

$$(\bar{\lambda}_\xi)_{i,j} = \phi_{i,j}(r)(\lambda_\xi)_{i,j} \tag{17a}$$

$$\phi_{i,j}(r) = 1 + r_{i,j}^\zeta \tag{17b}$$

where r is the ratio λ_η/λ_ξ, λ_ξ and λ_η are the scaled spectral radii of the flux Jacobian matrices (associated with the ξ and η directions) for the Euler equations, and the exponent ζ is generally taken to be 2/3. The spectral radii for the ξ and η directions are given by

$$\lambda_\xi = | uy_\eta - vx_\eta | + c\sqrt{y_\eta^2 + x_\eta^2} \tag{18}$$

$$\lambda_\eta = | vx_\xi - uy_\xi | + c\sqrt{x_\xi^2 + y_\xi^2} \tag{19}$$

and c is the speed of sound. The coefficients $\epsilon^{(2)}$ and $\epsilon^{(4)}$ use the pressure as a sensor for shocks and stagnation points, and they are defined as

$$\epsilon^{(2)}_{i+\frac{1}{2},j} = \kappa^{(2)} \max(\nu_{i-1,j}, \nu_{i,j}, \nu_{i+1,j}, \nu_{i+2,j}) \tag{20}$$

$$\nu_{i,j} = \left| \frac{p_{i-1,j} - 2p_{i,j} + p_{i+1,j}}{p_{i-1,j} + 2p_{i,j} + p_{i+1,j}} \right| \tag{21}$$

$$\epsilon^{(4)}_{i+\frac{1}{2},j} = \max[0, (\kappa^{(4)} - \epsilon^{(2)}_{i+\frac{1}{2},j})] \tag{22}$$

where $\kappa^{(2)}$ and $\kappa^{(4)}$ are constants. For the normal direction η, the dissipation contributions are defined in a similar way, except

$$(\bar{\lambda}_\eta)_{i,j} = \phi_{i,j}(r^{-1})(\lambda_\eta)_{i,j} \tag{23}$$

Elements of Numerical Algorithms

The system of differential equations [Eq. (12)] are advanced in time toward the steady-state solution with a five-stage

Runge-Kutta scheme. This scheme is second-order accurate in time. At the $(q+1)$ stage

$$W^{(q+1)} = W^{(0)} - \alpha_{q+1}\frac{\Delta t}{\Omega}\left[Q(W^{(q)}) - \sum_{r=0}^{q}\gamma_{qr}D(W^{(r)})\right] \quad (24a)$$

$$Q(W^{(q)}) = Q_c(W^{(q)}) + Q_d(W^{(0)}) \quad (24b)$$

where $W^{(0)}$ is the solution at time level n, α_{q+1} are the coefficients of the scheme, Δt is the time step, and γ_{qr} are the weighting factors of the artificial dissipation. The subscripts c and d refer to convection and physical diffusion contributions to the discrete terms of the flow equations. The coefficients α_{q+1} are determined such that the scheme has the largest possible hyperbolic stability limit. An appropriate set of coefficients is given by

$$\alpha_1 = 1/4, \quad \alpha_2 = 1/6, \quad \alpha_3 = 3/8, \quad \alpha_4 = 1/2, \quad \alpha_5 = 1$$

This scheme also exhibits good high-frequency damping behavior, which is crucial for a rapidly convergent multigrid method. In order to establish a good parabolic stability, the artificial dissipation terms are evaluated on the first, third, and fifth stages. The weighting factors γ_{qr} must satisfy the condition

$$\sum\gamma_{qr} = 1 \quad (25)$$

They are defined as follows:

$$\gamma_{00} = 1,$$

$$\gamma_{10} = 1, \quad \gamma_{11} = 0,$$

$$\gamma_{20} = \Gamma_3, \quad \gamma_{21} = 0, \quad \gamma_{22} = \bar{\gamma}_3,$$

$$\gamma_{30} = \Gamma_3, \quad \gamma_{31} = 0, \quad \gamma_{32} = \bar{\gamma}_3, \quad \gamma_{33} = 0,$$

$$\gamma_{40} = \Gamma_3\Gamma_5, \quad \gamma_{41} = 0, \quad \gamma_{42} = \bar{\gamma}_3\Gamma_5, \quad \gamma_{43} = 0, \quad \gamma_{44} = \bar{\gamma}_5 \quad (26)$$

where $\Gamma_3 = (1-\bar{\gamma}_3)$, $\Gamma_5 = (1-\bar{\gamma}_5)$, $\bar{\gamma}_3 = 0.56$, and $\bar{\gamma}_5 = 0.44$. As indicated in Eqs. (24), the physical viscous terms are computed only on the first stage and frozen for the remaining stages. The single evaluation appears to have no significant effect on the stability of the scheme and allows a reduction in computational effort. It is also important to note that the Runge-Kutta scheme has the desirable property that the steady-state solution is independent of the time step; therefore, the scheme is particularly amenable to convergence acceleration techniques.

Three methods are employed to accelerate convergence of the basic explicit time-stepping scheme. These techniques are 1) local time stepping, 2) implicit residual smoothing, and 3) multigrid. With local time stepping, the solution at each mesh point is advanced at the maximum Δt allowed by stability. Both convection and diffusion stability limits are included in the computation of Δt. Implicit smoothing of the residuals is used to extend the stability range of the basic time-stepping scheme. For two-dimensional problems, the residual smoothing can be applied in the form

$$(1-\beta_\xi\nabla_\xi\Delta_\xi)(1-\beta_\eta\nabla_\eta\Delta_\eta)\bar{R}^{(m)} = R^{(m)} \quad (27)$$

where the residual $R^{(m)}$ is defined by

$$R^{(m)} = \alpha_m\frac{\Delta t}{\Omega}[Q(W^{(m-1)}) - D^{(m)}] \qquad m = 1,5 \quad (28)$$

and computed in the Runge-Kutta stage m, $D^{(m)}$ is the total artificial dissipation at stage m, and $\bar{R}^{(m)}$ is the final residual at stage m after the sequence of smoothings in the ξ and η directions. The coefficients β_ξ and β_η are variable and functions of the spectral radii λ_ξ and λ_η. Referring to Refs. 2 and 7, they can be written as follows:

$$\beta_\xi = \max\left\{\frac{1}{4}\left[\left(\frac{CFL}{CFL^*}\frac{\lambda_\xi}{\lambda_\xi+\lambda_\eta}\phi(r)\right)^2 - 1\right], 0\right\} \quad (29a)$$

$$\beta_\eta = \max\left\{\frac{1}{4}\left[\left(\frac{CFL}{CFL^*}\frac{\lambda_\eta}{\lambda_\xi+\lambda_\eta}\phi(r^{-1})\right)^2 - 1\right], 0\right\} \quad (29b)$$

where $\phi(r)$ and $\phi(r^{-1})$ are the same quantities defined for the artificial dissipation, CFL is the local Courant number (usually taken to be 7.5), and the asterisk refers to the unsmoothed scheme.

The multigrid methods used with the CC and CV schemes (based on the work of Jameson[8]) are similar. For the multigrid process, coarser meshes are obtained by eliminating every other mesh line in each coordinate direction. With the CC scheme, the solution is transferred to coarser meshes by a rule that conserves mass, momentum, and energy. Simple injection is used with the CV scheme. Residuals are transferred from fine to coarse meshes by a weighted average.[8] A forcing function is constructed and introduced into the time-stepping scheme so that the solution on a coarse mesh is driven by the residuals collected on the next finer mesh. This process is repeated on each succeeding coarser mesh until the coarsest mesh is reached. Then, the corrections are transferred to the next finer mesh by bilinear interpolation. A fixed W-type cycle is used to execute the multigrid strategy. In order to make this strategy effective for a wide range of flow conditions, the resultant coarse grid corrections are smoothed before they are passed to the finest mesh. The factored scheme of Eq. (27) with constant coefficients ($\beta_\xi = \beta_\eta \approx 0.2$) is used for this smoothing. Also, the application of a full multigrid (FMG) method provides a well-conditioned starting solution for the finest mesh being considered. Finally, additional robustness of the multigrid schemes can be achieved by computing more than a single time step on the coarse meshes (see Ref. 7). This was not done in the present work.

Turbulence Model

The two-layer algebraic eddy viscosity model of Baldwin and Lomax[9] is used for turbulence closure. In order to improve the numerical compatibility of this model, two simple modifications were made. First, in the van Driest damping factor, which is used in the inner-layer eddy viscosity, the shear stress at the wall is replaced with the maximum local laminar shear stress. This generally prevents numerical difficulties due to vanishing shear stress at separation. Moreover, it removes the deficiency in the model where the turbulence

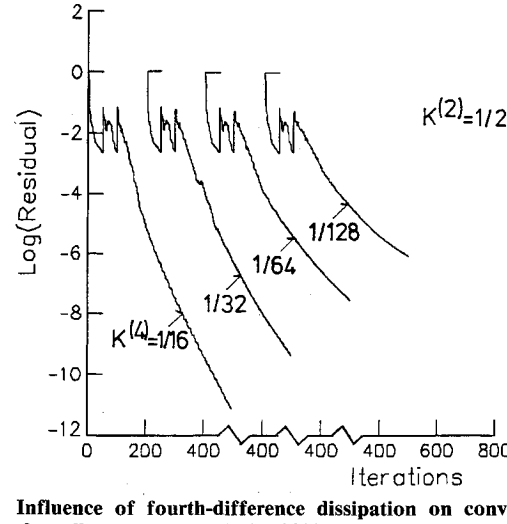

Fig. 3 Influence of fourth-difference dissipation on convergence behavior for cell vertex scheme (RAE 2822 airfoil, $M_\infty = 0.73$, $\alpha = 2.79$ deg, $Re = 6.5 \times 10^6$, grid -385×65).

becomes zero at separation. Second, the constant C_{WK}, which is used in the outer-layer eddy viscosity, is changed from 0.25 to 1.0. If this value is too low in the case of transonic flows, convergence may not be possible, due to motion of the shock wave. As indicated in Ref. 7, these changes result in only minor variations in airfoil flow solutions.

Results

The cell centered and cell vertex multigrid schemes described herein have been applied to a wide variety of airfoil flows. In this section, the accuracy and convergence behavior of these schemes are examined by considering computational results for transonic flows over the RAE 2822 airfoil. For the first calculation, designated case 9 in Ref. 10, the freestream Mach number (M_∞) is 0.73, the Reynolds number (Re_∞), based on chord, is 6.5×10^6, and the angle of attack (α) is 2.79 deg. The other set of flow conditions ($M_\infty = 0.75$, $Re_\infty = 6.2 \times 10^6$, $\alpha = 2.81$ deg) are referred to as case 10. Case 10 is one of the more difficult cases considered at the Viscous Transonic Airfoil Workshop of 1987.[11]

In Fig. 3, the influence of the fourth-difference dissipation on convergence behavior for the CV scheme is shown. Note that the residual of the continuity equation is reduced 10 orders of magnitude in less than 600 cycles using a moderate amount of artificial dissipation. Figure 3 also indicates the robustness of the computer code. That is, the dissipation coefficient is varied by nearly an order of magnitude without destroying the convergence of the scheme. The CC scheme responds in a similar manner to changes in dissipation.

The variation of the coefficients for lift, pressure drag, and friction drag with number of mesh points N is presented in Fig. 4. The effect of the fourth-difference dissipation is also indicated. For sufficiently fine meshes, one observes a linear variation of the coefficients with the product of the spacings Δx and Δy, as determined by $1/N$. Such a behavior not only indicates second-order accuracy (provided the slope is $O(1)$ in magnitude) but also permits simple extrapolation to obtain the infinitely fine mesh values. On coarse meshes (i.e., 193×33, $N^{-1} \approx 1.57 \times 10^{-4}$), the discretization error is dominated by artificial dissipation. The finer meshes allow the extrapolation of coefficients to their values for infinitely fine mesh. For the 385×65 mesh ($N^{-1} \approx 4.00 \times 10^{-5}$), the predicted lift is within 1.5%, the pressure drag is within 3 counts, and the

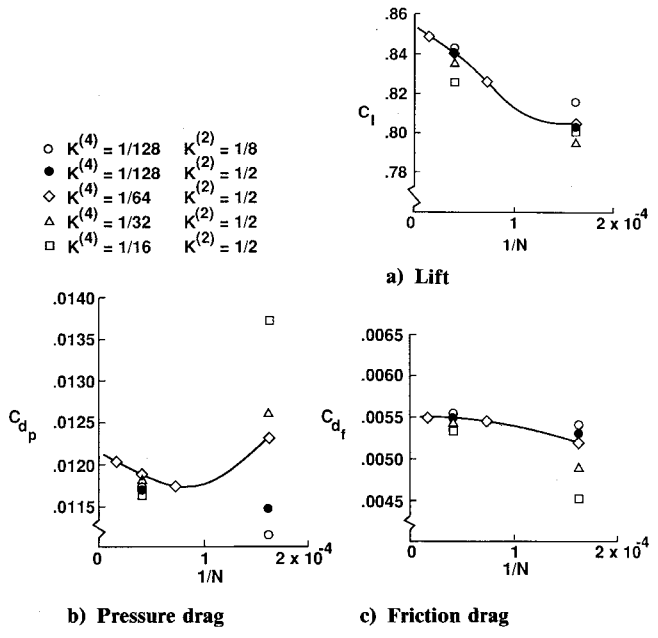

Fig. 4 Influence of grid density and artificial viscosity on global force coefficients for flow around RAE 2822 airfoil ($M_\infty = 0.73$, $\alpha = 2.79$ deg, $Re = 6.5 \times 10^6$), computed with cell vertex scheme.

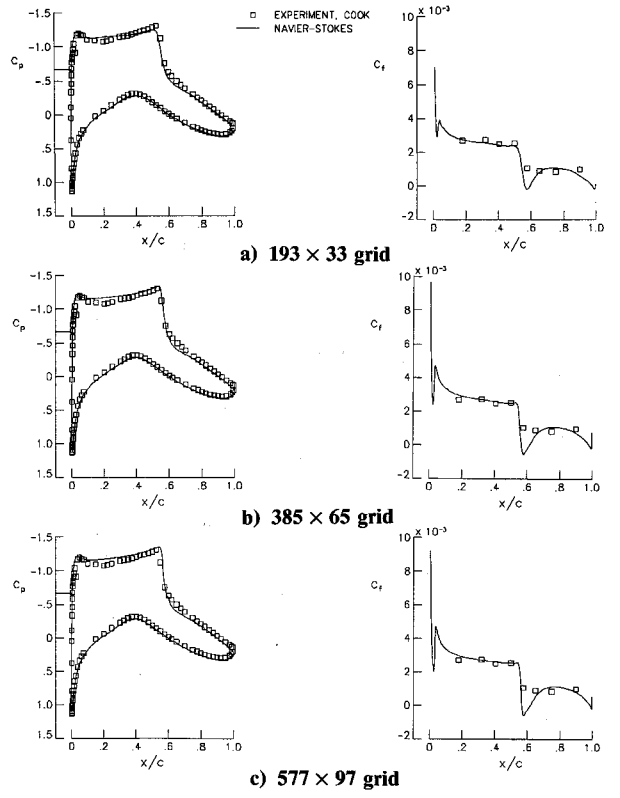

Fig. 5 Distributions of pressure and skin friction for different grid densities computed with cell vertex scheme (RAE 2822 airfoil, $M_\infty = 0.73$, $\alpha = 2.79$ deg, $Re = 6.5 \times 10^6$, $\kappa^{(4)} = 1/64$).

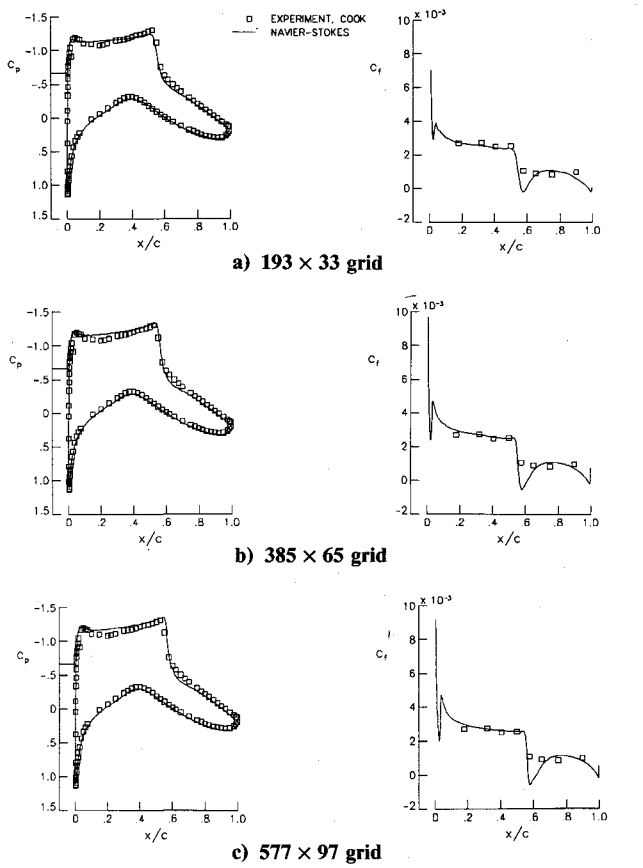

Fig. 6 Distributions of pressure and skin friction for different grid densities computed with cell centered scheme (RAE 2822 airfoil, $M_\infty = 0.73$, $\alpha = 2.79$ deg, $Re = 6.5 \times 10^6$, $\kappa^{(4)} = 1/64$).

Table 1 Mesh parameters

Grid	$\Delta y_{\min}$	Δs_{le}	$\Delta x_{x=0.5c}$	Δx_{te}	SF
193×33	2.25×10^{-5}	7.31×10^{-3}	4.45×10^{-3}	1.83×10^{-2}	1.56
385×65	1.00×10^{-5}	3.40×10^{-3}	2.13×10^{-3}	9.43×10^{-3}	1.25
577×97	6.67×10^{-6}	1.64×10^{-3}	1.04×10^{-3}	4.78×10^{-3}	1.16

friction drag is within 0.1 count of the extrapolated values. For the 577 × 97 mesh ($N^{-1}\approx1.79\times10^{-5}$), the lift is within 0.5%, the pressure drag is within 1 count, and the friction drag is within about 0.1 count of the infinitely fine mesh values.

Figures 5 and 6 show pressure and skin-friction distributions for different grid densities. In Table 1, the following parameters are defined for each mesh: the minimum normal spacing ($\Delta y_{\min}$); the streamwise spacing at the leading edge (Δs_{le}), the midchord of the upper surface ($\Delta x_{x=0.5c}$), and the trailing edge (Δx_{te}); the normal stretching factor (SF). There is close agreement between the results computed with the CC and CV schemes. Observe that the main features of the flow are essentially captured with the 193 × 33 mesh. Also, with only 33 points in the normal direction, a good approximation of the skin-friction distribution is obtained. There are only small differences between the 385 × 65 mesh solution and the 577 × 97 mesh solution. All of the skin-friction curves show a sudden rise at the airfoil trailing edge. Such behavior is nonphysical and a consequence of artificial dissipation and turbulence modeling. By the application of strong scaling of the streamwise numerical dissipation in the immediate vicinity of the trailing edge, the abrupt skin-friction rise can be essentially eliminated (see Ref. 6).

The distributions in surface pressure and upper surface skin friction obtained for case 10 with the two multigrid schemes are compared in Fig. 7. Again, the solutions exhibit only minor differences. In each computation, the predicted shock location is downstream of the experimental one. This result is

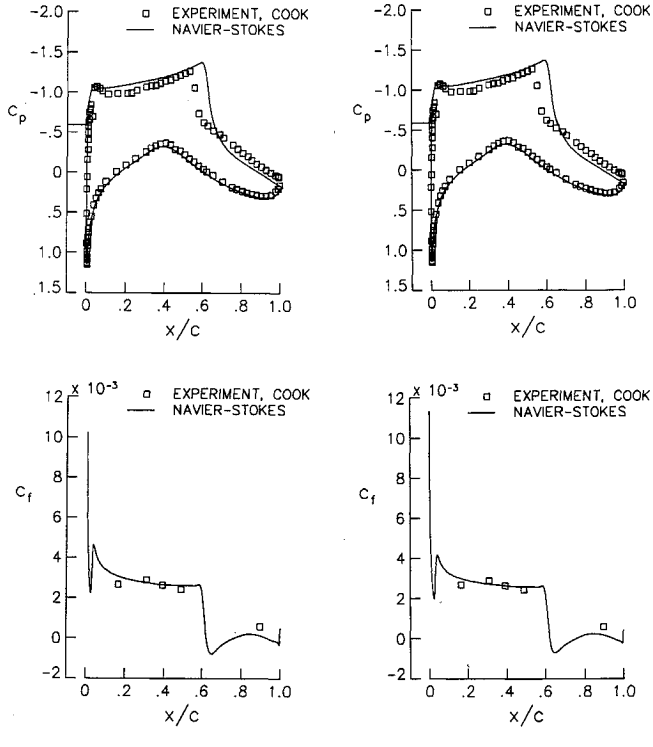

a) Cell centered scheme ($c_l = 0.8404$, $c_d = 0.0284$)

b) Cell vertex scheme ($c_l = 0.8395$, $c_d = 0.0285$)

Fig. 7 Comparison of cell centered and cell vertex schemes for flow around RAE 2822 airfoil ($M_\infty = 0.75$, $\alpha = 2.81$ deg, $Re = 6.2 \times 10^6$, grid − 385 × 65, $\kappa^{(4)} = 1/64$).

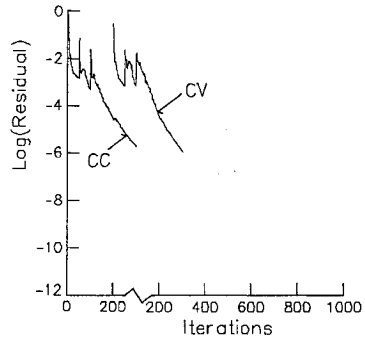

Fig. 8 Comparison of the convergence behavior of cell centered and cell vertex schemes for flow around RAE 2822 airfoil ($M_\infty = 0.73$, $\alpha = 2.79$ deg, $Re = 6.5 \times 10^6$, grid − 385 × 65, $\kappa^{(4)} = 1/64$).

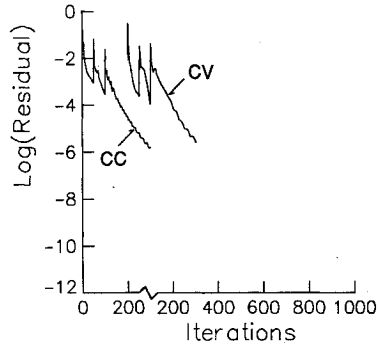

Fig. 9 Comparison of the convergence behavior of cell centered and cell vertex schemes for flow around RAE 2822 airfoil ($M_\infty = 0.75$, $\alpha = 2.81$ deg, $Re = 6.2 \times 10^6$, grid − 385 × 65, $\kappa^{(4)} = 1/64$).

a consequence of the breakdown in the turbulence equilibrium assumption (production and dissipation are balanced) of the algebraic turbulence model used in the calculations. For case 10, there is a much stronger interaction of the shock wave with the boundary layer than for case 9. Moreover, there is separation, or nearly so, over about the last 40% of the upper surface of the airfoil. This situation requires modeling of the convection of turbulence, at least in the outer region of the turbulent boundary layer where there is a slower response to the adverse pressure gradient. In other words, the "history" effects of turbulence must be modeled. As shown in Ref. 12, the correct shock position can be computed for case 10 by applying a turbulence model (i.e., Johnson-King model) that accounts for the nonequilibrium effects.

A comparison of convergence histories for the CC and CV schemes is displayed in Figs. 8 and 9. For both cases 9 and 10, the convergence behavior of these schemes is very similar. The CV scheme has a somewhat faster asymptotic convergence rate. This appears to be due to differences in the treatment of boundary conditions. Convergence to engineering accuracy is achieved with each scheme in about 75 multigrid cycles with the finest mesh (385 × 65). This corresponds to about 2 min CPU time on the CRAY II computer.

Concluding Remarks

A cell centered scheme and a cell vertex scheme for the Navier-Stokes equations, which are based on central-difference approximations and Runge-Kutta time stepping, have been described. Using local time stepping, implicit residual smoothing, a multigrid method, and carefully designed artificial dissipation terms, very good convergence rates are obtained for both schemes. In general, engineering accuracy is obtained within 75 multigrid cycles on the fine mesh. An analysis of discretization error indicates that the cell vertex scheme should exhibit smaller discretization errors on stretched meshes. Numerical results show that the two computer codes give almost identical results for transonic airfoil

flows, even on coarse meshes. The error introduced by the numerical dissipation terms is apparently larger on coarse meshes than the discretization error of the physical terms.

The grid refinement study, which is presented in this paper, allows an extrapolation of computed lift and drag to their values on an infinitely fine mesh. Thus, a quantitative estimate of the errors in lift and drag for finite-grid density can be determined.

Acknowledgment

The present work evolved while the second author stayed at NASA Langley Research Center. The help of C.-C. Rossow, who provided the cell vertex Euler code as a basis for the present study, is gratefully acknowledged.

References

[1]Swanson, R. C., and Turkel, E., "A Multistage Time-stepping Scheme for the Navier-Stokes Equations," AIAA Paper 85-0035, Jan. 1985.

[2]Martinelli, L., "Calculations of Viscous Flows with a Multigrid Method," Ph.D. Dissertation, MAE Dept., Princeton Univ., Princeton, NJ, Oct. 1987.

[3]Radespiel, R., and Rossow, C., "A Cell Vertex Finite Volume Scheme for the Two-Dimensional Navier-Stokes Equations," DFVLR-IB 129-87/40, Braunschweig, Germany, Dec. 1987.

[4]Morton, K. W., and Paisley, M. F., "A Finite Volume Scheme with Shock Fitting for the Steady Euler Equations," Oxford Univ. Computing Lab. Rept. 87/6, Oxford, England, UK, July 1987.

[5]Jameson, A., Schmidt, W., and Turkel, E., "Numerical Solutions of the Euler Equations by Finite Volume Methods Using Runge-Kutta Time-Stepping Schemes," AIAA Paper 81-1259, June 1981.

[6]Swanson, R. C., and Turkel, E., "Artificial Dissipation and Central Difference Schemes for the Euler and Navier-Stokes Equations," *Proceedings of the AIAA 8th Computational Fluid Dynamics Conference,* AIAA, New York, 1987, pp. 55–69.

[7]Arnone, A., Swanson, R. C., "A Navier-Stokes Solver for Cascade Flows," NASA-CR 181682, July 1988.

[8]Jameson, A., "Multigrid Algorithms for Compressible Flow Calculations," Princeton Univ., Princeton, NJ, MAE Rept. 1743 (text of lecture given at 2nd European Conf. on Multigrid Methods, Cologne, Germany, Oct. 1985).

[9]Baldwin, B. S., and Lomax, H., "Thin Layer Approximation and Algebraic Model for Separated Turbulent Flows," AIAA Paper 78-257, Jan. 1978.

[10]Cook, P. H., McDonald, M. A., and Firmin, M. C. P., "AEROFOIL RAE 2822 Pressure Distributions, and Boundary Layer and Wake Measurements," AGARD Advisory Rept. 138, May 1979.

[11]Holst, T. L., "Viscous Transonic Airfoil Workshop Compendium of Results," AIAA Paper 87-1460, June 1987.

[12]Coakley, T. J., "Numerical Simulation of Viscous Transonic Airfoil Flows," AIAA Paper 87-0416, Jan. 1987.